Chapter 1

Reweighting Dynamics in full Conformational Space

This chapter focuses on testing the reweighting scheme introduced in section **??** on minimal models where the full conformational space is known. The models consist of a single particle so entropic effects due to many-body interactions are absent. This provides a minimal testing ground for the reweighting method. The first with changing potential surface tests for the special case of equilibrium systems. The second systems extends to NESS by a global external force with periodic boundary conditions, introduced in section **??**. The third system is inspired by a laser model and applies non-conservative forces locally [3]. The forth model tests the global driving on a 2 dimensional single particle.

External forces are applied to push the system in a NESS. An external reservoir at constant temperature is connected to control fluctuations and withdraw excess heat. The systems are simulated using molecular dynamics for 10 different driving forces and a MSM is constructed. One system is reweighted continuously in other systems and checked if dynamical and static information from simulation are recovered correctly. The static information are tested by the stationary distribution, the dynamical information are tested by the first-passage-time distribution between metastable states (see section **??**). Only chosen processes are compared by full FPTD, because comparison of all FPTD with each other is cumbersome. The systems are compared by the first three moments of the FPTD and the metastable state occupation probabilities. The reweighting test is considered successful if all information are recovered

correctly.

The presented results for all models except the 2D model were published in [1].

1.1 Single Particle in 1D Potential Well

The potential shown in figure 1.1 is a 1D potential of type shown in section **??** with diverging boundaries and three wells. The applied force in positive direction can be described by an additional potential $U_{\text{ext}}(x) = -fx$ that tilts the existing potential. The diverging boundaries prevent the system to enter a NESS and restrict the system to equilibrium. Equilibrium is a case of a NESS with 0 entropy production on average and the dynamics are governed by detailed balance. This ensures that the heat dissipated moving a particle between two points in space does not depend on the chosen trajectory. This effect simplifies the description of dynamics considerably. The reweighting procedure is designed for general NESS so the assumptions of the reweighting method are met. The model will serve as a first testing ground to test the precision of the reweighting scheme. The MSM was constructed with a lagtime 0.004 $\mathcal{T}$ and 60 microstates.

The static and dynamic properties for the system without potential tilting and with maximum tilting at $f = 9\ \frac{\epsilon}{\mathcal{L}}$ is shown in figure 1.1. The presented FPTD from state C to B slows down significantly with increasing tilting. Transition times above 50 τ are previously rare and become likely in the new potential. The reweighting procedure recovers this detailed view on the dynamics exactly. Previously unknown trajectories are captured by the reweighting correctly.

Figure 1.2 presents the first three moments and the occupation probability of the metastable states. The potential is constructed such that two processes have the same FPTD in equilibrium. These are the processes $A \to B$ and $C \to B$ going from left and right inwards to the central potential, processes $B \to A$ and $B \to C$, their inverse processes going outwards from the central potential. Processes $A \to C$ and $C \to A$ crossing the whole system via state B and can be seen as a combination of two processes. The additional force breaks the symmetry and speeds up the processes in the direction of the force, while inverse processes are slowed down. The variance of the distributions show the same behavior as the MFPT, a larger mean allows larger variation. The skewness is stable at $\approx 2\tau^3$, except for the process $A \to B$. This

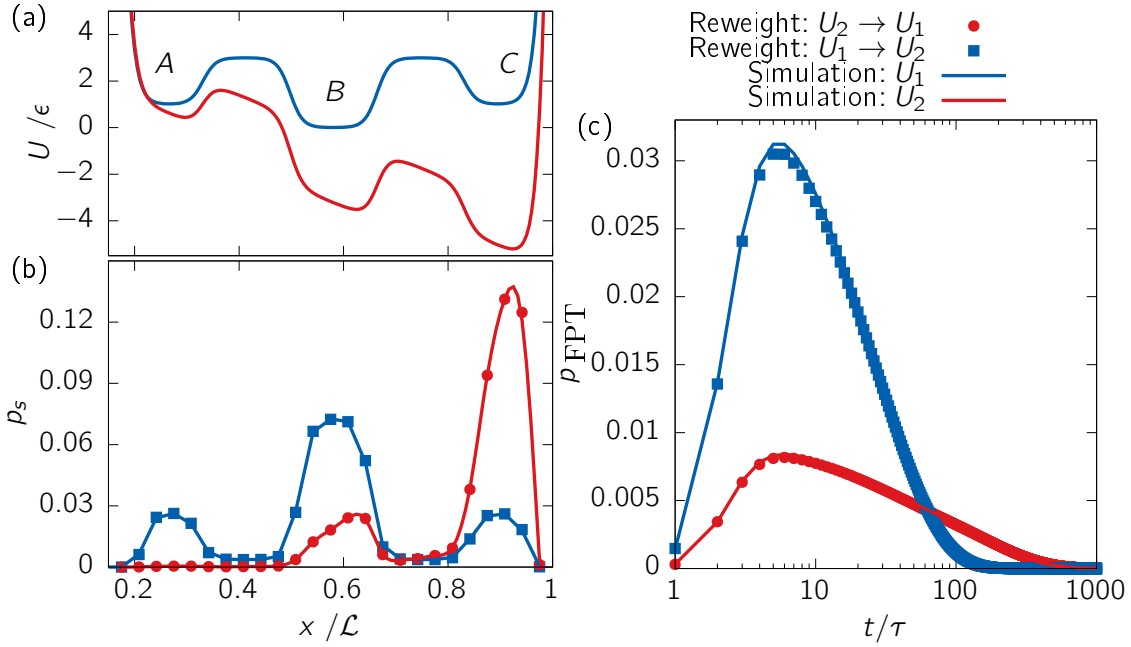

Figure 1.1: (a) Potential, (b) stationary distribution and (c) FPTD of the process $C \to B$. The lines in (b,c) represent the results from simulating the system potentials, the dots are the results from reweighting the systems into each other. A, B, C mark the metastable states. The system without tilting is represented blue, the system with tilting in red.

process is increasingly fast, such that it is described by processes of time-length of the lagtime τ, as shown in figure 1.1c. A increased growth of processes faster than the distribution mean result in increasing skewness. Smaller lagtime of the MSM would shift this effect to higher driving forces. All processes are still captured correctly, so there is no need to change the initial construction of the MSM.

Reweighting continuously from the equilibrium system shows the precision of the method over the range of driving forces. Furthermore, the driven states between the simulated ones can be explored without further simulation. It is concluded that the reweighting method recovers static and dynamic properties without further simulation for the special case of equilibrium systems. We will turn to the class of all NESS in the next section.

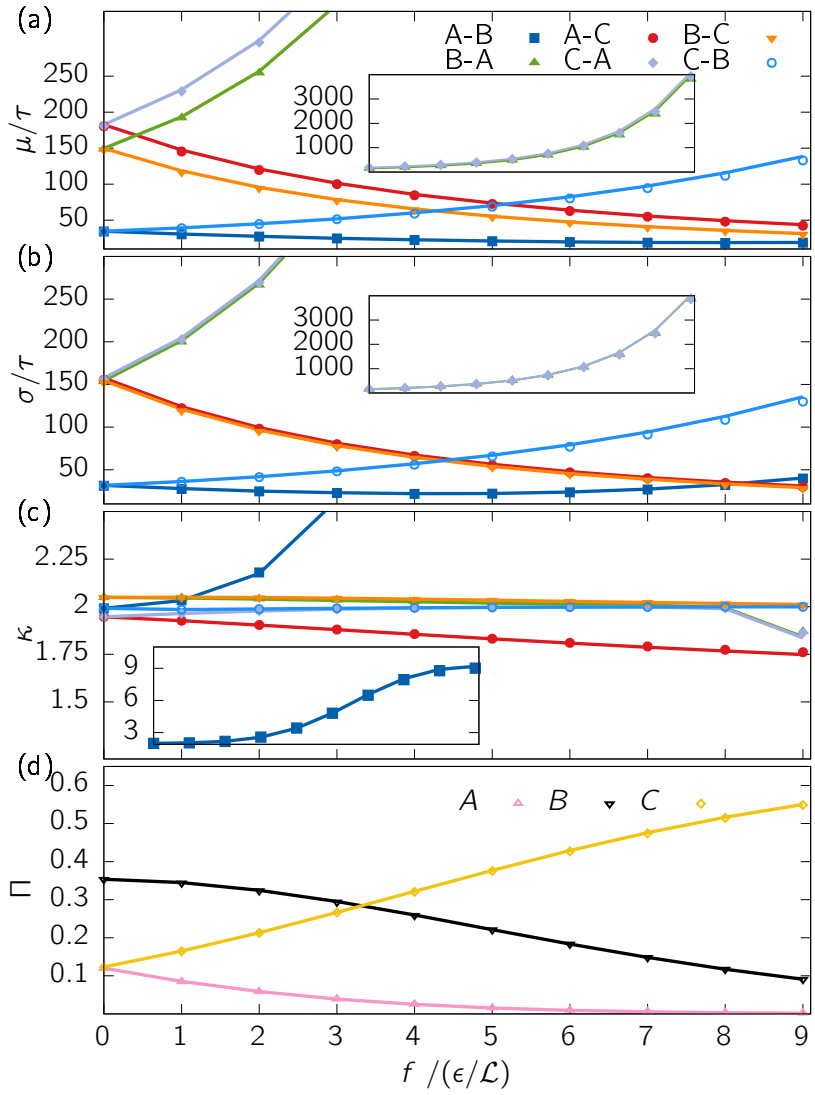

Figure 1.2: $(a-c)$ The first three moments of the FPTD for all six processes between metastable states in figure 1.1 under varying tilting of the potential. (d) The occupation probability of each metastable state. The dots represent the value measured from simulation. The line is the equilibrium system continuously reweighted.

1.2 Single Particle in 1D under Global Driving

A single particle in 1D periodic-boundary potential is driven in one direction by an external force. Since the particle has a preferred direction to move the dynamics do not fulfil detailed balance. The external force cannot be described by a potential. The heat dissipated to move the particle between two space-points becomes path dependent. In particular, the heat dissipated depends on the particle moving between two points in space along a trajectory with or against the external force. This is a minimal example to describe a NESS. The reweighting scheme will be shown to capture the path-dependence of the dynamics correctly.

The corresponding MSM describing the dynamics is constructed from simulation data in detail in section **??** with a lagtime $\tau = 0.002\ \mathcal{T}$ and 60 microstates. The reference potential surface with non-conservative forces is shown in figure 1.3a. The diverging potential at the boundaries of the equilibrium system in the previous section 1.1 was replaced by a potential barrier of height 5 ϵ. The stationary distribution and a FPTD for a chosen process without driving and a system driven by $9\frac{\epsilon}{\mathcal{L}}$ are shown in figure 1.3b,c. The systems are reweighted into each other. The simulation and reweighting data match precisely for the stationary distribution and the FPTD from state C to B.

The potential shown in figure 1.3a represents the equilibrium system without driving force. The direction of the force is marked in red and applied over the whole system with equal strength. The first three moments of the FPTD for all involved slow processes and the stationary distribution of metastable states is shown in figure 1.5. The processes $A \to B$ and $B \to C$ are aligned with the external force and become faster. The process $C \to A$ shows abnormal behaviour by slowing down first and speeding up at force $> 4\ \frac{\epsilon}{\mathcal{L}}$. For the equilibrium system, the connection via state B is spatially longer but more probable than the direct connection over the large barrier. Both sets of trajectories are presented by two peaks in the FPTD in figure 1.4. This weighting of path changes under driving until the jump over the large barrier between the states becomes more probable for increasing driving. At this point, the process speeds up with increasing force. The process $B \to A$ opposing the external force slows down first. After the jump over the barrier between state A and C becomes more probable, the transition $B \to A$ benefits from using new transition trajectories via state C and increases speed. The transition $C \to B$ slows down against the force. We can expect that it changes trend for larger forces too. The variances show a similar behaviour as the MFPT as seen for the previous system. The skewness is

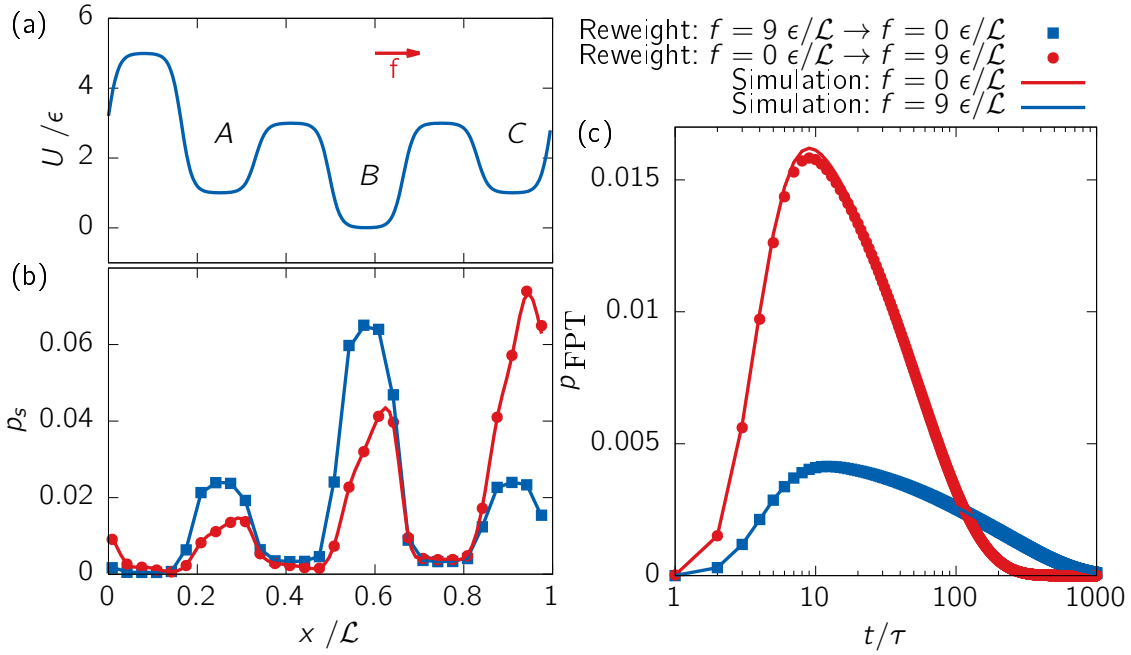

Figure 1.3: (a) Potential and external force (b) stationary distribution and (c) FPTD of the process $C \rightarrow B$. The lines in (b,c) represent the results from simulating a single particle in the potential without (blue) and with (red) external force. The dots are the results from reweighting the systems into each other. A, B, C mark the metastable states.

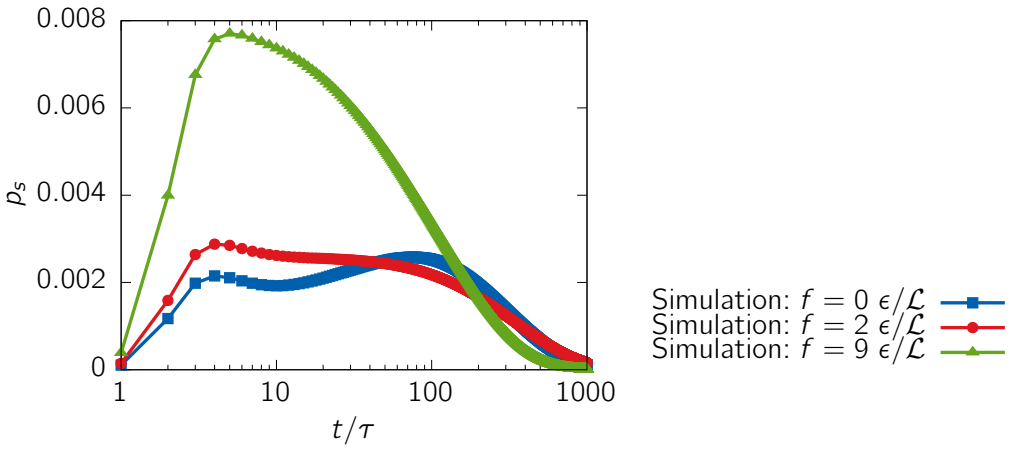

Figure 1.4: FPTD of transition $C \rightarrow A$ simulated at 3 different driving forces. The equilibrium system at $f = 0$ is a bimodal distribution, indicating two sets of trajectories for that trajectory. The two peaks merge to one as driving increases. One set of trajectories is suppressed by the driving.

more variable, but stays in a range of $\approx 2\tau^3$. The skewness of transition $A \rightarrow B$ increases due to its strong increase in short-term processes again. The increase is less than for the previous system, because a lower lagtime for the MSM was chosen. The occupation probability changes over driving such that state B becomes higher populated than state C for driving $> 4\ \frac{\epsilon}{\mathcal{L}}$. This is an off-equilibrium effect where population of high energy states is higher than the population of low energy states. This effect is called *population inversion* [6] and is impossible in equilibrium because populations follow Boltzmann statistics.

The previous discussion shows that the current minimal system shows complex non-equilibrium behaviour by introducing path-dependence to the system. This path-dependence of transition breaks the monotonous increase/decrease in MFPT under driving from the equilibrium system by promoting one collection path over another. This is not possible in a equilibrium system. Additionally population inversion is achieved by breaking detailed balance: A probability flow from one state of the system is allowed without a symmetric back-flow, irrespective of the stationary distribution. Global balance makes sure that the probability flows away in other direction so probability flow is conserved.

The presented method shows perfect results for the case of NESS. We will now test

the boundaries of the driving and the effect of local driving.

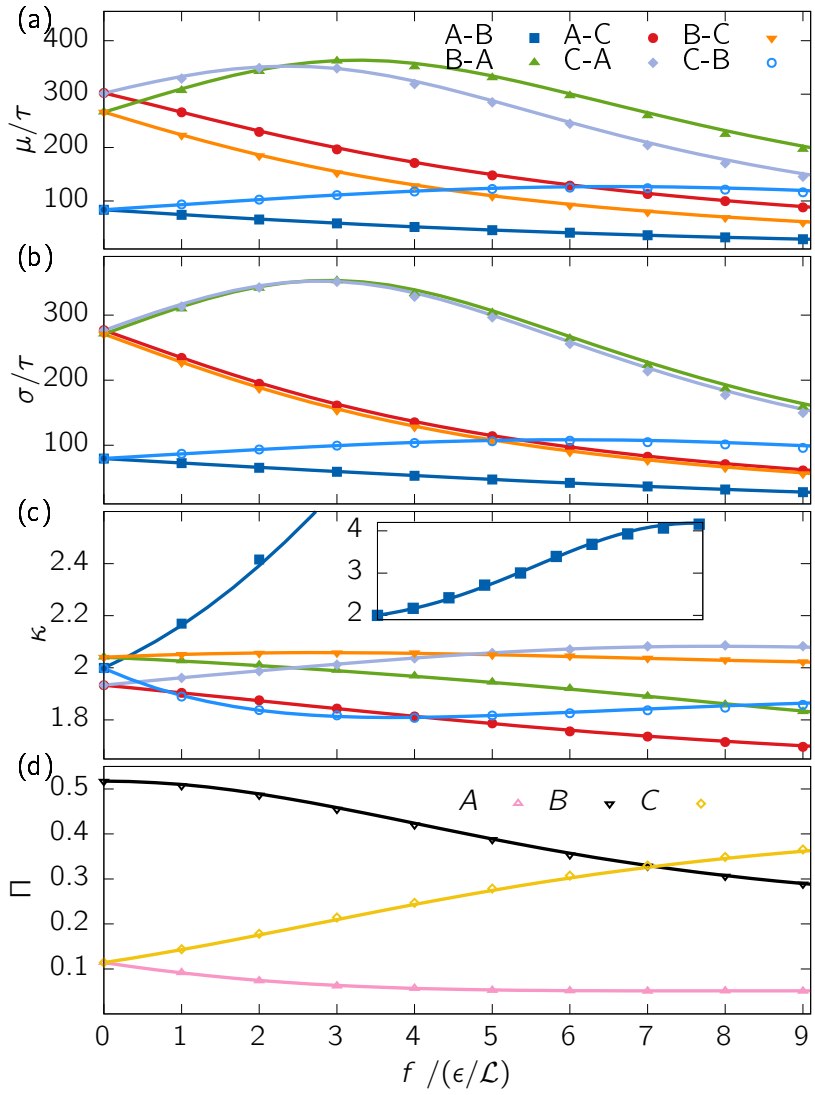

Figure 1.5: (a-c) The first three moments of the FPTD for all six processes between metastable states in figure 1.3 under varying external force f. (d) The occupation probability of each metastable state. The dots represent the value measured from simulation. The line is the equilibrium system continuously reweighted.

1.3 Single Particle in 1D under Local Driving

This model is inspired by a laser model with 4 states. A laser is in a far-off-equilibrium steady state and shows population inversion where high energy electron states are more populated than low energy states [2]. Relaxing electrons from the high energy state to a low energy state emits photons. The steady state is driven by an external force pumping electron to higher energetic states. The laser starts emitting monochromatic light when the higher energy states are more populated than the lower states.

An electron in figure 1.6 starting in state A is pushed to the highest energetic state B by absorption of energy. Typically this energy is provided by optical illumination and photon absorption, chemical reactions or electronic discharge [2]. In this simplified model, the driving is represented by a Gaussian shaped force irrespective of the source. From the highest state, it relaxes fast to a state C with slightly lower energy under emission of heat in form of vibrations to surrounding atoms. This state is used to depopulate state B, so it can be repopulated quickly by the pumping. The electron relaxes from state C to D by emitting a photon. In practice this may happen by spontaneous or stimulated emission. The relaxation from state D to A is fast under the emission of vibrational energy to surrounding atoms like the transition $B \to C$. The depopulation of state D will promote the desired transition $C \to D$. Direct transitions between non-neighbouring states like $B \to D$ are forbidden by the selection rules of quantum mechanics. All described transition may occur the other way round by random fluctuations. The pumping will promote the described path and suppress the inverse path. Without this pumping, the forward and backward transition becomes equal likely, i.e. the system fulfils detailed balance and Boltzmann statistics apply. The flow in cycles is essential for a NESS. That means a 3-state laser model can be constructed by deleting supporting states B or D and it can show population inversion too. A 2-state laser would automatically fulfil detailed balance and cannot show population inversion.

The model is not designed to be an accurate presentation for a laser. The helium-neon-laser for example uses 3 states of the helium and 6 states of the neon gas [5]. The number of states, the barriers and energy levels are chosen purely phenomenological. The transition states are modelled by a steep potential slope and the classical Langevin equation do not represent quantum mechanical transitions. There is only a single particle in the system, i.e. the electron are non-interacting. The model is designed to achieve a complete population inversion, where the equilibrium occupa-

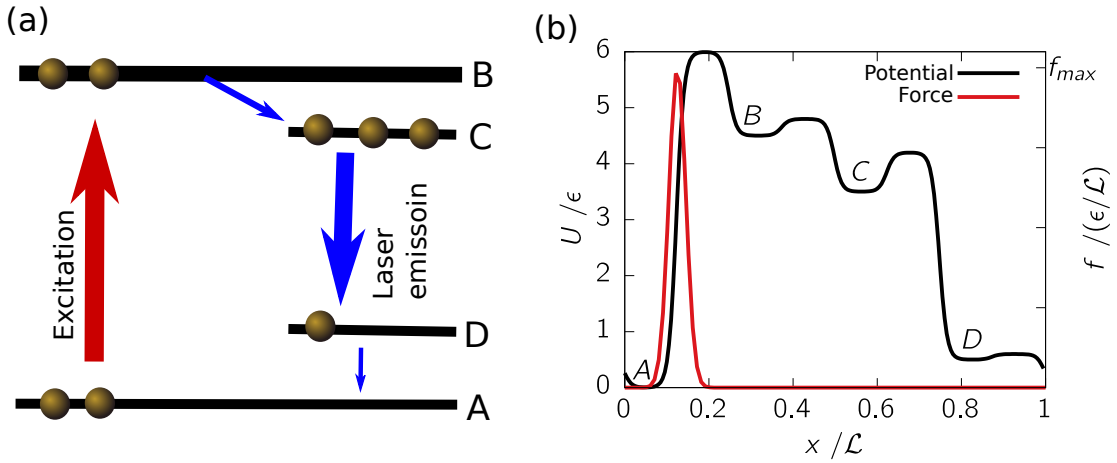

Figure 1.6: (a) Sketch of a 4-state laser model. The electron are pumped from state A to state B, marked by the red arrow. the blue arrows represent relaxation transition. The transition $C \to D$ relaxes under emission of a photon. (b) Translation of laser model (a) to a continuous potential surface. The excitation is represented by a Gaussian force directed up the potential barrier.

tion order is inverted for all four states. It shows that the equilibrium and driven states share less dynamics than in the previous system. This tests the boundaries of the reweigthing procedure because it requires reliable reference data. Furthermore, the reweighting procedure is tested on external forces that act locally.

The MSM was constructed with 64 microstates and a lagtime of $0.002\mathcal{T}$. The equilibrium system and a system driven at peak force $200\frac{\epsilon}{\mathcal{L}}$ is compared in figure 1.7. It should be noted that the peak force is 20 times higher than external forces used in previous system. The stationary distributions are completely inverted by this force, the high energy state is highest populated and the low energy state minimally. The stationary distribution are recreated well by the reweighting procedure. There is a small artifact at the peak of the external force for the reweighted driven system. The FPTD is shown for the pumped transition from A to B. The short-time processes are more probable by a factor of 10 for the pumped process compared to the equilibrium process. The equilibrium system shows transition over the whole spectrum from 10 to 10000 MSM steps. The reweighting procedure recovers the FPTD for both systems well although transition duration differs by a factor of 10.

The comparison for different driving forces by the first three moments of the FPTD

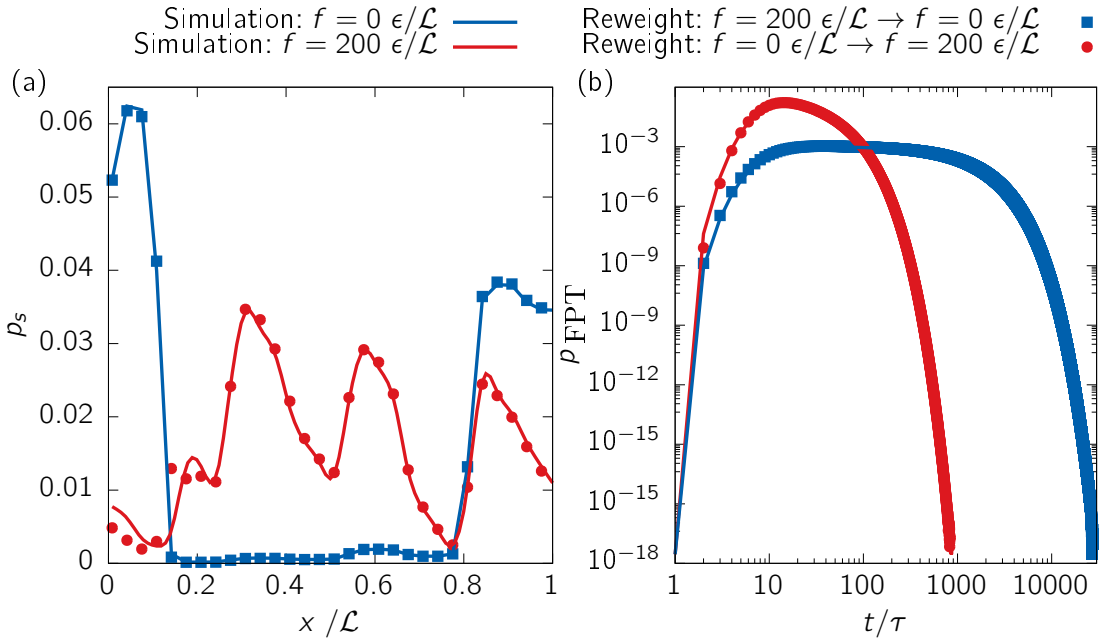

Figure 1.7: (a) stationary distribution and (b) FPTD of the excitation process $A \to B$. The lines in (a,b) represent the results from simulating a single particle in the potential without (blue) and with (red) external force. The dots are the results from reweighting the systems into each other.

and the metastable state population is shown in figure 1.8. The analysis shows the pumping and emission transition and their corresponding inverse transition. Note the logarithmic scale in mean and variance to capture the large differences in timescales of the observed systems. The MFPT of the pumping transition $A \to B$ speeds up drastically as desired. The inverse pumping transition is affected much less and the mean increases slowly. The relaxation transition $C \to D$ is unaffected by the pumping. The inverse relaxation $D \to C$ speeds up with the pumping caused by the cyclic motion via A and B, not by a direct jump. Again, the variance follows the behaviour of the mean, also in magnitude. The skewness does not show any new behaviour, the skewness of transition $A \to B$ is increasing again when approaching low MFPT. The stationary distribution shows the first population inversion of state B and C for $f > 70\epsilon/\mathcal{L}$. The populations are globally inverted for $f > 170\epsilon/\mathcal{L}$.

Simulation and reweighting from equilibrium agree well, but some deviation can be seen for increased driving. Major deviations occurs in the MFPT and the skewness of the NESS of transition $A \to B$ for driving $f > 150\epsilon/\mathcal{L}$. The MFPT is underestimated due to the defect in stationary distribution shown in figure 1.7. This can be an effect of the discretisation of state. The localised Gaussian force is continuous in simulation and discretised in the reweighting procedure, where it spreads out over just a few microstates in the MSM. We observe that the local error does not effect other transitions. The large deviation in skewness is connected to the previously described effect for very low MFPT. The reweighting procedure can capture localised forces but the microstates should be chosen fine so the discretised description of the forces is sufficient. Most of the deviations occur when the driving is very large compared to previous driving forces. The method relies on sufficient data from the reference simulation. The underlying dynamics of both processes are so different that deviations can occur because the reference sampling is noisy, similar to the effect of missing reference data in equilibrium reweighting (see section **??**). Furthermore, the MSM was constructed for the equilibrium system. The dynamics of the driven system are much faster and the lagtime can be too large to describe the system properly. Considering these effects, deviations for heavy driving are in an acceptable range.

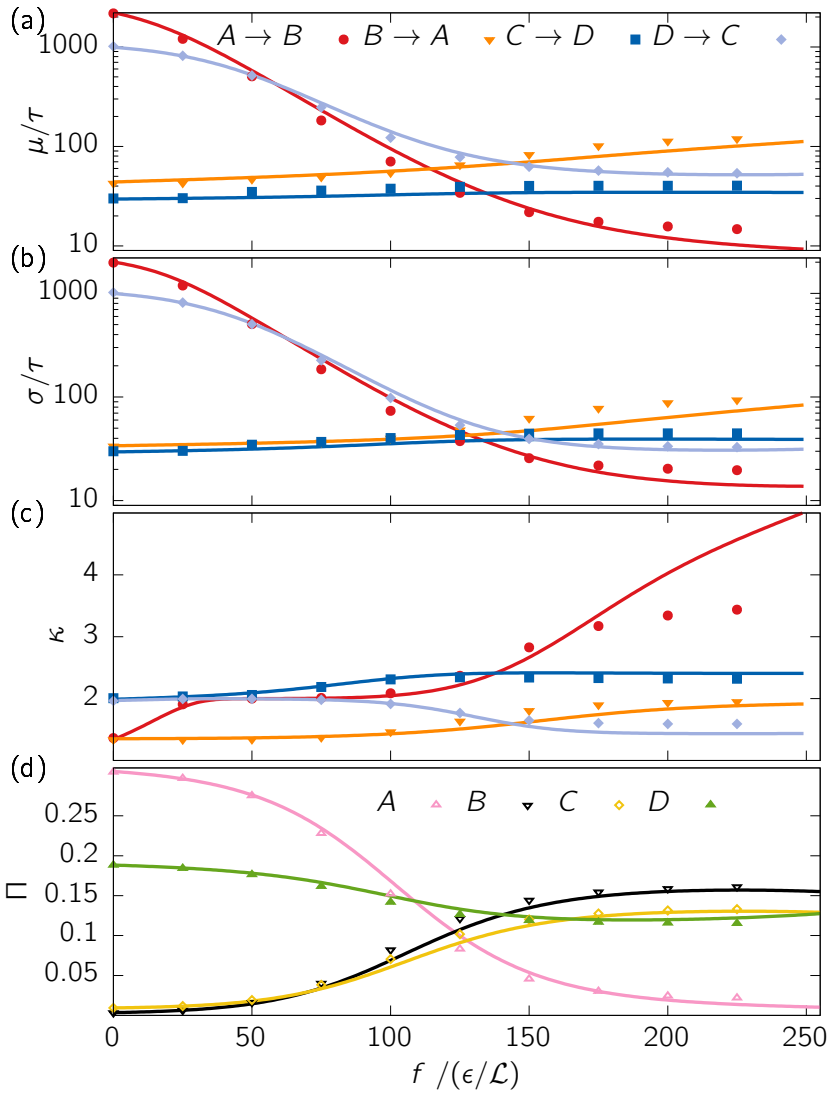

Figure 1.8: (a-c) The first three moments of chosen FPTD between metastable states in figure 1.7 under varying external force f. The transition are the pumping transition $A \to B$ and the emission transition $C \to D$ with both inverse transitions. (d) The occupation probability of each metastable state. Full population inversion for driving $f > 170\epsilon/\mathcal{L}$. The dots represent the value measured from simulation. The line is the equilibrium system continuously reweighted.

1.4 Single Particle in 2D under Global Driving

The non-interacting particle is suspended in a 2D potential to introduce a second degree of freedom that has to be recovered correctly. The configuration space increases quadratically and challenges the reweighting method by a large number of microstates.

The potential consists of three Gaussian potential wells of varying depth, shown in figure 1.9a. All boundaries are periodic and the external force is applied along the x-direction. The microstates consists of 30x10 squares of equal size, the lagtime was chosen at $0.02\mathcal{T}$. The potential minima were chosen at 3ϵ, 5ϵ ,and 7ϵ, located on a line in the middle of the y-axis. The standard deviation of the Gaussian is $0.02\mathcal{L}$ in both directions.

A detailed view on a driven system is given in figure 1.9. The simulated system at $9\frac{\epsilon}{\mathcal{L}}$ and the reweighted system agree in probability distribution at first sight. Figure 1.9b adds the probabilities distribution for a y-value along the middle of the system with highest probability, one at boundary of the system with lowest probability distribution and one medium, comparing the simulated and reweighted stationary distribution. The logarithmic scale reveals a deviation when reweighting from equilibrium to the driven system. The probability density around the minima decreases with driving and more states surrounding the minima are occupied. Within the basins, the distribution is tilted in the direction of the force. The occupation probabilities between the basins are estimated too low and too high in the minima. This error was not identified for the 1D-systems and it is more pronounced in the driven than in the equilibrium system. The FPTD of the transition $C \to B$ peaks at faster processes for the driven system because the transition via A becomes more prominent. The equilibrium transition occur at a broader probability peaking between $10 - 30\tau$. A small deviation between simulation and reweighting can be seen at the peak of the driven distribution. The process speeds up by a factor of 10.

The first three moments of the six slowest FPTD and the metastable state occupation probability is shown in figure 1.11. The MFPT becomes faster for all processes under driving. Only the processes $C \to B$ and $B \to A$ slow down for small driving before speeding up. Similar to the 1D system in section 1.2, this can be explained by an initial slowing down by the particles taking the direct path against the force. For larger driving the spatially longer paths along the external force become more prominent and increase speed of the process. Compared to the 1D system under

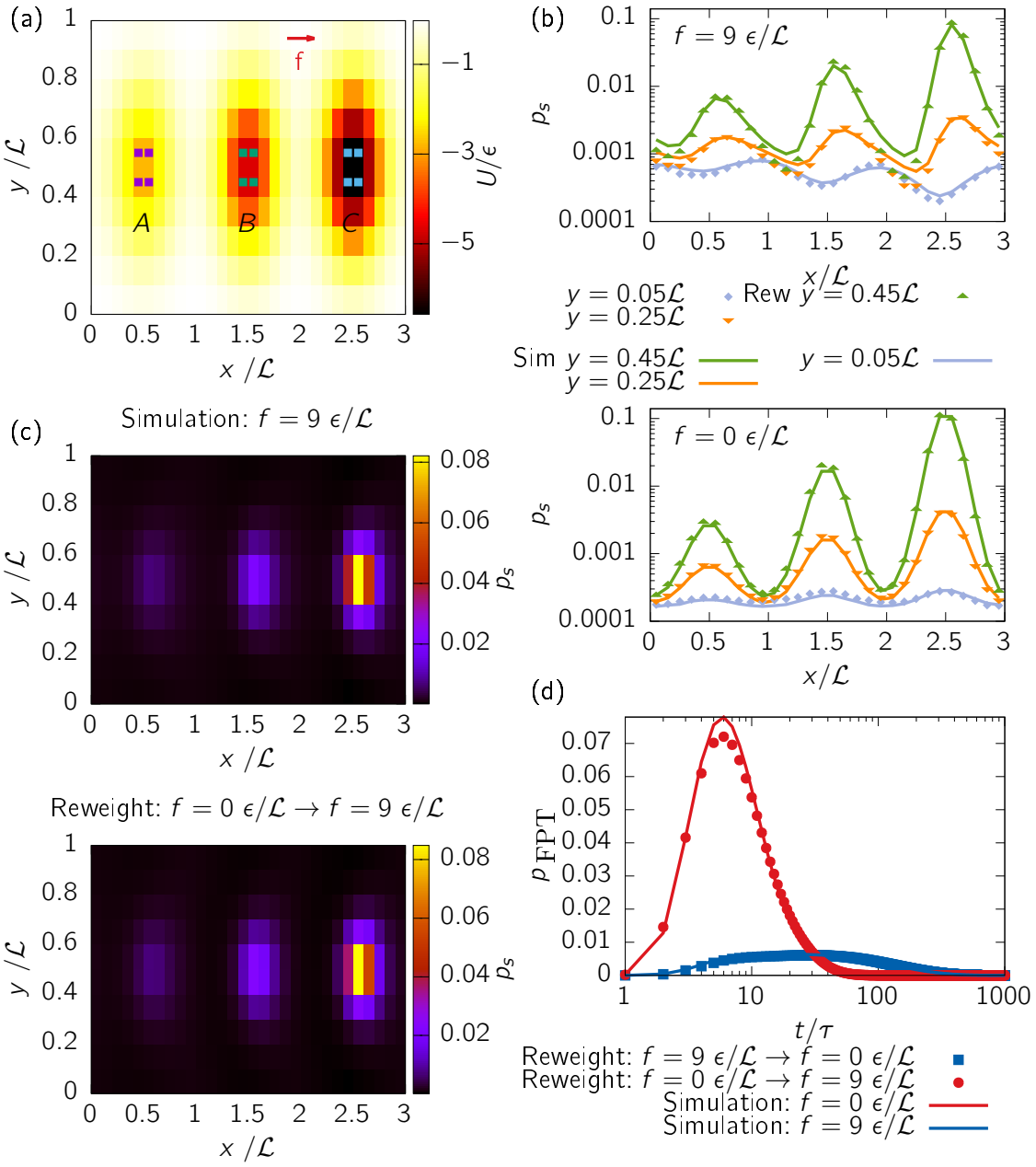

Figure 1.9: (a) The potential surface with the metastable states marked A, B, C. (b) Stationary distribution under driving from simulation and from reweighting. (c) Detailed view on the stationary distribution in equilibrium and driven with $9\frac{\epsilon}{\mathcal{L}}$ on states with $y = 0.05\mathcal{L}, 0.25\mathcal{L}, 0.45\mathcal{L}$. The lines are the results from simulation, the dots from reweigthing into each other. (d) FPTD of the process $C \to B$. The lines represent the results from simulating a single particle in the potential without (blue) and with (red) external force. The dots are the results from reweighting the systems into each other.

global driving, this phenomena comes into effect for much lower driving although the potential barriers are larger. A possible reason is the bypassing of the intermediate state because the potential barriers are small close to the y-boundaries, because all Gaussian are centered in y-direction. The increase in occupation probability in y-direction means that more trajectories pass by these states. Again, the variance shows the same trend as the MFPT. The skewness levels around ≈ 2 again. The process $A \to B$ shows abnormal behaviour by increasing until $4\frac{\epsilon}{\mathcal{L}}$ and then decreasing again. The skewness of process $A \to C$ on the other hand becomes smaller than usual. Both effects can be explained with another set of slower processes entering the system for increasing driving: The potential in A is a too weak obstacle for the particle flowing by. There is an increasing probability that they simply bypass the metastable state lying in the minimum of the potential and produce trajectories longer than the system size. The effect is shown in figure 1.10 where increased driving of process $A \to B$ results in an increase of short-time processes on the left-hand-side of the distribution. Further driving produces a second small peak on the right-hand-side, showing the long-time processes bypassing A. The decrease in MFPT is slowing down and the skewness decreases by this effect. The bypassing can only occur for a 2D system. The metastable state occupation in figure 1.11 of state C decreases and occupation of state A and B stay approximately the same. The depopulation of the highest probability state was seen in the 1D system too. The other states do not increase in population because the probability generally spreads out from the potentials minima. A broader definition of metastable states would capture this in an increase of occupation probability with increasing driving.

The reweighting technique shows good results for this model too. We can see some deviation, e.g. for the peak of the FPTD in figure 1.9d or the occupation probability between the basins in figure 1.9. Both effects only take place when reweighting over a broad range of driving. The additional degree of freedom an larger number of microstates is a challenging task for the reweighting procedure and gives insight in its possible limitations. In particular we find that states away from the basins are not recovered correctly by the reweighting. The sources of deviation for all systems will be discussed in detail in the next chapter.

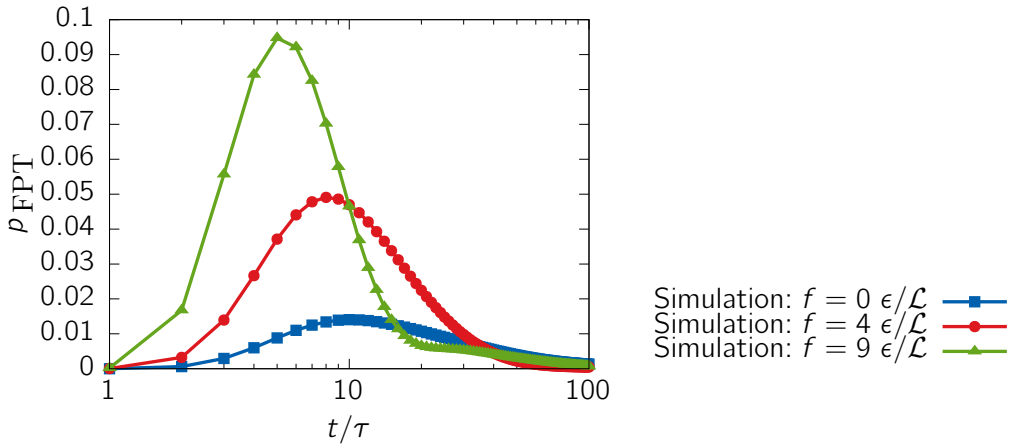

Figure 1.10: FPTD of transition $A \rightarrow B$ simulated at 3 different driving forces. Increased driving promotes short-time processes and suppresses slow processes. For $f = 9\frac{\epsilon}{\mathcal{L}}$ a second peak appears at $\approx 30\tau$, showing new long-term processes.

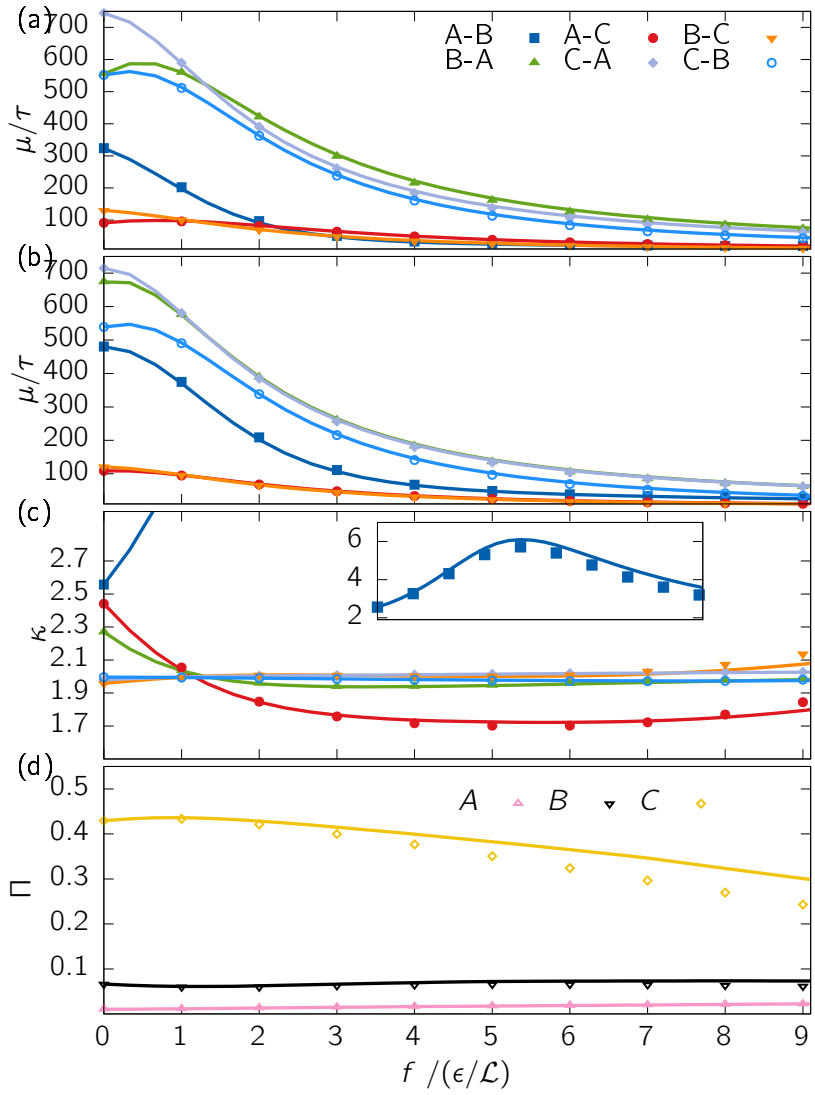

Figure 1.11: (a-c) The first three moments of the FPTD for all six processes between metastable states in figure 1.9 under varying external force f. (d) The occupation probability of each metastable state. The dots represent the value measured from simulation. The line is the equilibrium system continuously reweighted.

1.5 Discussion

The previous sections applied the reweighting scheme to a number of different systems, all being single particles in different external potentials under varying driving forces. The potential surface and the external forces can be varied locally once a MSM for a reference system was created. The gathered information can be reweighted to any other system, as long as it is similar to the reference system. This section discusses the precision and limitation of this method.

The method needs two sets of input data: Any reference data in form of a MSM and the local entropy production of the target system. The latter can be included by the total entropy production ΔS_{ij} from state i to j or by the difference in entropy production of reference and target system $\Delta S_{ij} - \Delta S_{ij}^q$ as shown in equation **??**. Any system can be chosen for a reference, indicating that there is an underlying Invariance in the reference systems, as it was introduced in equation **??**. This physical meaning of the invariant is further discussed in section **??**.

The method relies on sampling transition probabilities of a system sufficiently. The underlying simulated trajectories give a more detailed picture but are broken into pieces of local transitions. Sampling the transition probabilities is a much easier task than sampling complete trajectories. As a result trajectories that were not sampled in the reference system are constructed by the MSM of the reweighted system. This can be seen in the FPTD for all systems (see figure 1.1, 1.3 , 1.7, 1.9), when long trajectories are created although they were not sampled in the reference system. The underlying MSM allows us to construct trajectories that are important in the target system. This is a fundamental difference to the Ferrenberg-Swendsen reweighting for equilibrium introduced in section **??**: The method fails if states required in the target system are not sufficiently sampled in the reference system. Translated to dynamics it means that the important transition probabilities of the target system have to be sampled sufficiently in the reference system. The complete trajectories do not need to overlap because they can be constructed afterwards. The locality of the entropy productions is key for the system to work because each part of the trajectory is reweighted individually to constitute the local nature of non-equilibrium processes. The global balance and normalisation account for the interaction of all microtransition.

1.5.1 Sources of Error

The FPTD shows small deviations from its expected distribution with increasing reweighting distance. This deviation is largest in the peaks of the distribution and for the stationary distribution of the 2D system in figure 1.11. Error analysis was performed on different systems to exclude sampling issues. Other sources of the deviation are possible and are discussed in the following:

- The approximation was used in the deviation of the reweighting formula
- Insufficient constraints in the Maximum Caliber
- Chosen microstates and lagtime of reference MSM might be unsuitable for target system
- Limitation for large fluctuations

The necessity of the approximation was discussed in detail in section **??**. The exact set of equations emerging from the Caliber cannot be solved numerically. Furthermore the full set of equation may have more than one solution and it cannot be guaranteed to find the correct one. The approximation solves this issue by having a singular solution and fulfilling the constraints of the Caliber. The significance of this error cannot be determined without a full solution available.

Constraining the Caliber according to the local entropy production was based on the model how the system interacts with its environment. Global balance was introduced to model the internal connection of the states. Success of the method is based on the quality of the constraints. It cannot be excluded that other effects play a major role. If other effects exist they are minor for the given systems. If one can be identified it can be included in the Caliber. For now we assume the set of constraint to be complete.

Another source of error is based on the construction of the Markov State Model. The microstates are chosen equi-sized and independent of data so all models can be represented by it. The lagtime on the other hand is chosen based on a method requiring equilibrium data (see section **??**). The method fails for NESS so the lagtime of the reference equilibrium system is assumed to be valid for the target system too. When reweighting over large distances this assumption might be flawed. An indicator

Technical Point 1.1 The Kramers Model

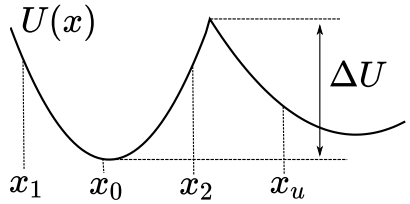

The Kramers model [4] describes non-dissipative dynamics of molecular reactions by a 1-dimensional potential $U(x)$ coupled to a head-bath at temperature T with coupling constant γ. It estimates the rate of a transitioning over a barrier by

$$k = \frac{k_\mathrm{B}T}{\gamma}\left(\int_{x_0}^{x_u}\exp\left(\frac{U(x)}{k_\mathrm{B}T}\right)\int_{x_1}^{x_2}\exp\left(\frac{-U(x)}{k_\mathrm{B}T}\right)\right)^{-1}$$

The first integral is over the transition region, the second integral captures the starting potential or the initial probability distribution. Kramers showed how the transition rate depends on the form and the height of the potential. It requires that the equilibration time τ_e in one basin is much smaller than the transition times $\tau_t \gg \tau_e$. To be consistent we have to assume that $k_\mathrm{B}T \ll \Delta U$.

is the MFPT that changes considerably e.g. for the laser system. This suggests a change in timescale and the lagtime of the target MSM might be chosen inconsistent with the markovian assumption. The user has to reweight MSMs constructed at different lagtimes to check for deviations based on this issue.

The method is limited to systems where fluctuations are not stronger than the potential surface. Tests showed that potential barriers of $\Delta U < k_\mathrm{B}T$ are not captured well by the reweighting method. The random fluctuation take over the system-dependent local entropy productions. The barrier crossing dynamics are governed by the local potentials and captured well (see technical point 1.1). The diffusion dynamics governed by symmetric fluctuations on the other hand are not well captured. This effect can be seen in the 2D system in figure 1.11 where trajectories bypass some potential minima for heavy driving. The potential barrier close to the boundary in y-direction are often smaller than kinetic energy from fluctuations. Once these states show larger population, the error becomes more pronounced. The presented errors for heavy driving might emerge from this limitation of the method.

The mentioned sources of errors are oftentimes difficult to check. However, this chapter shows that the errors are minimal compared to the range of the reweighting method. Even increasing/decreasing the speed of processes by the order of 10 is captured with minor deviation. A full error analysis on the construction of the Markov State Model or developing a minimisation algorithm for the full solution of

the Caliber can be useful for future investigation. The presented data proves the concept of Maximum Caliber minimisation under constraining global balance and local entropy production for reweighting MSM between NESS.

Bibliography

[1] Marius Bause, Timon Wittenstein, Kurt Kremer, and Tristan Bereau. Microscopic reweighting for nonequilibrium steady-state dynamics. *Physical Review E*, 100(6):060103, 2019.

[2] Michael Kaschke, Karl-Heinz Donnerhacke, and Michael Stefan Rill. *Optical devices in ophthalmology and optometry: technology, design principles and clinical applications*. John Wiley & Sons, 2013.

[3] Ahsan U Khan and Michael Kasha. Mechanism of four-level laser action in solution excimer and excited-state proton-transfer cases. *Proceedings of the National Academy of Sciences*, 80(6):1767–1770, 1983.

[4] Hendrik Anthony Kramers. Brownian motion in a field of force and the diffusion model of chemical reactions. *Physica*, 7(4):284–304, 1940.

[5] Richard Leach. *Fundamental principles of engineering nanometrology*. Elsevier, 2014.

[6] Christian Maes. *Non-dissipative effects in nonequilibrium systems*. Springer, 2018.